LAJSBA
LATIN AMERICAN JOURNAL OF SEDIMENTOLOGY AND BASIN ANALYSIS | VOLUME 28 (2) 2021, 133-151

EVOLVING CONTROLS ON MINERALIZATION IN PATAGONIAN MICROBIAL MATS AS INFERRED BY WATER CHEMISTRY, MICROSCOPY AND DNA SIGNATURES

Inès Eymard [1], Maria del Pilar Álvarez [2], Andrés Bilmes [3], Crisogono Vasconcelos [4,5], Camille Thomas [1], Daniel Ariztegui [1]*

[1] Department of Earth Sciences, University of Geneva, Geneva, Switzerland.
[2] IPPEC-CONICET, Puerto Madryn, Chubut, Argentina.
[3] IPGP-CONICET, Puerto Madryn, Chubut, Argentina.
[4] ETH, Geologisches Institut, Zürich, Switzerland.
[5] CGA-SGB/CPRM, Rio de Janeiro, Brazil.
* daniel.ariztegui@unige.ch

ARTICLE INFO

Article history
Received October 7, 2021
Accepted December 20, 2021
Available online December 28, 2021

Handling Editor
Fernando Gómez

Keywords
Living microbialites
Organomineralization
Abiotic
Maquinchao Basin

ABSTRACT

In recent years resulting investigations in living microbialites have provided significant data that have been critical to disentangle the role of the various biotic and abiotic processes contributing to their development. Despite these efforts separating the impact and magnitude of these processes remain a difficult task.
At present the Maquinchao Basin in northeastern Patagonia, Argentina, contains both fossil and living microbialites. Thus, the region provides a unique opportunity to investigate the impact of intrinsic and extrinsic parameters in carbonate precipitation. Early investigations (Austral summer 2011) in living microbialites concluded that organomineralization was related to both photosynthetic activity in the more surficial layer (green), and sulfate-reduction in the lower part (beige). Field investigations in the same area four years later showed that the pounds previously containing abundant active mats had dried out, and in general revealed the absence of globular structured clusters of minerals in the microbial mats. Here we present microscale investigations using optical microscopy and SEM along with the 16SrRNA gene sequence diversity, and the physico-chemical parameters of the hosting waters. They were carried out in successive seasonal samplings in November 2015, April-May 2016, August 2016, February 2017, and March 2018. All microbialite samples show regular occurrences of sulfate reducing bacteria (SRB) along with filaments of unknown origin. Carbonates are observed associated with erect filaments in shallow and active running water locations whereas the mineral phase is located below organic matter film in comparatively deeper and calmer water areas. Additionally, seasonal changes in the physico-chemical properties of the hosting waters indicate that extrinsic parameters, especially evaporation, might play a more substantial role in the precipitation of these carbonates than previously proposed. The environmental differences between 2011 and 2015 in meteorological conditions, regional volcanic activity and associated deposits in the basin are analyzed. We concluded that they are likely responsible of the decrease of the mineralization processes, and particularly those associated with photosynthetic activity.
These results call for caution when interpreting the degree of biological impact

on the formation of microbialites in the geological record. Local extrinsic factors might have a changeable impact over time switching mineral precipitation from biotic to abiotic and vice-versa, which can be undistinguishable in fossilized microbialites.

INTRODUCTION

Microbial carbonates represent some of the earliest forms of life on Earth but disentangling the role of the various biotic and abiotic processes contributing to their development remains a difficult task. Significant advances have been achieved by studying their living counterparts, such as well-known modern stromatolites, microbial mats, and biofilms (Awramik and Riding, 1988; Reid *et al.*, 1995; Dupraz *et al.*, 2004; Casaburi *et al.*, 2015). The interaction between physicochemical parameters of the hosting waters and different microorganisms such as eukaryotes, prokaryotes, and more specifically bacteria, and their metabolic products have been demonstrated to play a substantial role in mineral precipitation (Visscher and Stolz, 2005; Dupraz *et al.*, 2009). The chemistry of the environment is further essential ruling the composition of the resulting minerals (Dupraz *et al.*, 2009). The metabolic activity of the microbial communities affects alkalinity and can either promote mineralization or dissolution of calcium carbonates (Dupraz *et al.*, 2009). Photosynthesis is likely the dominant process, however, is not the only metabolic process contributing to the precipitation of this mineral. Lyons *et al.* (1984) and Visscher and Stolz (2005) pinpointed the role of sulfate reduction increasing alkalinity and, therefore, promoting carbonate mineralization. However, whereas some microbial communities promote carbonate formation some others prevent it, such as aerobic heterotrophs and sulfide oxidizers whose metabolism can favor carbonate dissolution (Dupraz *et al.*, 2009). This process of mineral formation arising from a local increase of alkalinity related to the metabolism of microbial organisms is defined as *"biologically-induced"* organomineralization. However, organomineralization is not only induced, but can also be *"biologically-influenced"*. The latter implying an increase of alkalinity as a result of changes in certain environmental parameters. Physico-chemical processes such as CO_2 degassing by wave action, mixing of groundwater and lake water, and evaporation would lead to the precipitation of carbonate abiotically, using the microbial mats as substrate for precipitation (Pentecost, 2005). Hence the alkaline engine is key in the precipitation of carbonates that along with the lack of Ca^{2+} and/or HCO_3^- would change the undersaturation index (SI) preventing the precipitation of calcium carbonates. Often abiotic processes, also referred as extrinsic parameters (CO_2 degassing, evaporation, etc.), and biotic processes, referred as intrinsic parameters (photosynthesis, microbial organic matter degradation, other metabolic activities), are considered separately when trying to understand organomineralization. Their respective roles in the process of microbialite formation, however, must be collectively understood and amalgamated to interpret the geological and biological processes associated with their development.

The Maquinchao Basin in northwestern Argentinean Patagonia contains fossil and modern microbialites. Early investigations have already reported the presence of carbonate buildups and the most recent studies have focused mostly on the fossils by looking at their use as proxies in paleoenvironmental reconstructions (Galloway *et al.*, 1988; Whatley and Cusminsky, 1999; Ariztegui *et al.*, 2001; Schwalb *et al.*, 2002; Tatur *et al.*, 2002; Ariztegui *et al.*, 2008; Cartwright *et al.*, 2011) the impact of environmental parameters on the distribution of outcropping Pleistocene carbonate buildups at both mega and macro scales (Eymard *et al.*, 2019; 2020); and their evolution from formation to erosion by focusing on their microstructures and mineralogy.

Pacton *et al.* (2015) first observed in the Austral summer of 2011 mineralizing modern mats of globular macroscopic structure in the Maquinchao River. *In situ* parameters and major elements were measured in the hosting waters. Further laboratory studies in the living mats identified an upper green and a lower beige layer where most of the calcium carbonate cluster and mineralization were observed.

They were inspected using Transmission Electron Microscopy (TEM), Scanning Electron Microscopy (SEM) and Confocal Laser Scanning Microscopy (CLSM). Samples were stained for Fluorescence in situ Hybridization (FISH) observations through CLSM with focus on Sulfate Reducing Bacteria (SRB) and Cyanobacteria. The organomineralization was related to both photosynthetic activity in the green layer, and sulfate-reduction in the lower part (beige).

Field investigations in the same area four years later showed that the pounds previously containing abundant active mats had dried out, and in general revealed the absence of globular structured mats. However, a few mats could still be retrieved in one of the areas investigated by Pacton *et al.* (2015), but no cluster of minerals was observed. By investigating the basin four years after, this study seeks in pursuing the geomicrobiological investigation of active mats observed in 2011 to use these results as an analogue for the formation of the Late Pleistocene Maquinchao microbialites. Microscale investigations along with the 16SrRNA gene sequence diversity, and the physico-chemical parameters of the hosting waters are complementing Pacton *et al.* (2015) observations to improve our understanding of the differences in the distribution and morphology of these microbialites throughout the basin.

GEOLOGICAL AND GEOGRAPHICAL SETTINGS

The endoreic Maquinchao Basin is located in the Patagonian foreland, Rio Negro province, Argentina (41°08′S and 69°28′W). The area is a tectonic depression sitting at an elevation of ca. 800m a.s.l. surrounded by Miocene basaltic plateaus on east and west sides of the basin. Currently it encloses two shallow water lakes, Carri Laufquen Grande (CLG) and Carri Laufquen Chica (CLC), connected by the ephemeral Maquinchao River, partially sustained by groundwater (Fig. 1). The region is characterized by strong winds with regular speeds of ~100 km/hr (Argentinean Meteorological Service, 1981-2010; (Agosta *et al.*, 2015), and a dry climate with an annual mean precipitation of 200 mm/year. Rainfall from years 2000 to 2011 has decreased affecting the lake levels and river as well as the aquifers (Fig. 2). CLG and CLC have been described as hypersaline to brackish water and brackish to freshwater compositions, respectively (Pacton *et al.*, 2015). In this contribution we provide complementary data from sampling campaigns carried out in January 2011, November 2014, May 2016, August 2016 and February 2017 (Alvarez *et al.*, 2021). Satellite data indicate recent water level fluctuation for both lakes (Departamento Provincial de Aguas, DPA 2012; Bilmes *et al.*, 2019). Additionally, paleoshorelines have been reported in previous studies (Galloway *et al.*, 1988; Bradbury *et al.*, 2001; Cartwright *et al.*, 2011; Bilmes *et al.*, 2019) showing the large instability of this aquatic system at longer time scales.

The investigations by Pacton *et al.* (2015) first revealed the presence of modern mats, in different ponds of the Maquinchao River, composed of filamentous and coccoid bacteria as well as amorphous organic matter (OM). Low Mg calcite crystals ranging from 200nm to 500nm, were observed in the mats and associated with extracellular polymeric substances (EPS) in areas with active SRB, mostly located in the lower part of the mats. Four years later some of the pounds where active mats were first observed by Pacton *et al.* (2015) were dry while others had substantially diminished with the occurrence of fewer microbial mats (Fig. 1). Furthermore, the 2015 mats did not present the macroscopic globular texture and did not appear to be mineralized in locations B and C compared to those shown in Pacton *et al.* (2015) observations (Fig. 3, panel I) .

MATERIAL AND METHODS

Water sampling

Physicochemical parameters such as temperature, pH and electrical conductivity (EC) were measured *in situ* at all sampling locations, using a portable system (Lutron WA-2017SD). Water samples were taken to perform major elements analyzes. Additionally, a water monitoring sampling has been conducted during five field campaigns (November 2015, April-May 2016, August 2016, February 2017, and March 2018). Surface waters of both lakes CLG and CLC were collected when the shore was reachable as well as water samples from mats sampling sites (Carvallo Maquinchao). Furthermore, hand pits have been dug in and around the Maquinchao River to identify the groundwater flux (Alvarez *et al.*, 2021), and waters from other wells associated with Carvallo Maquinchao point (CLA 2P, CLA 3P) were collected. Pits were dug by hand until reaching the water table,

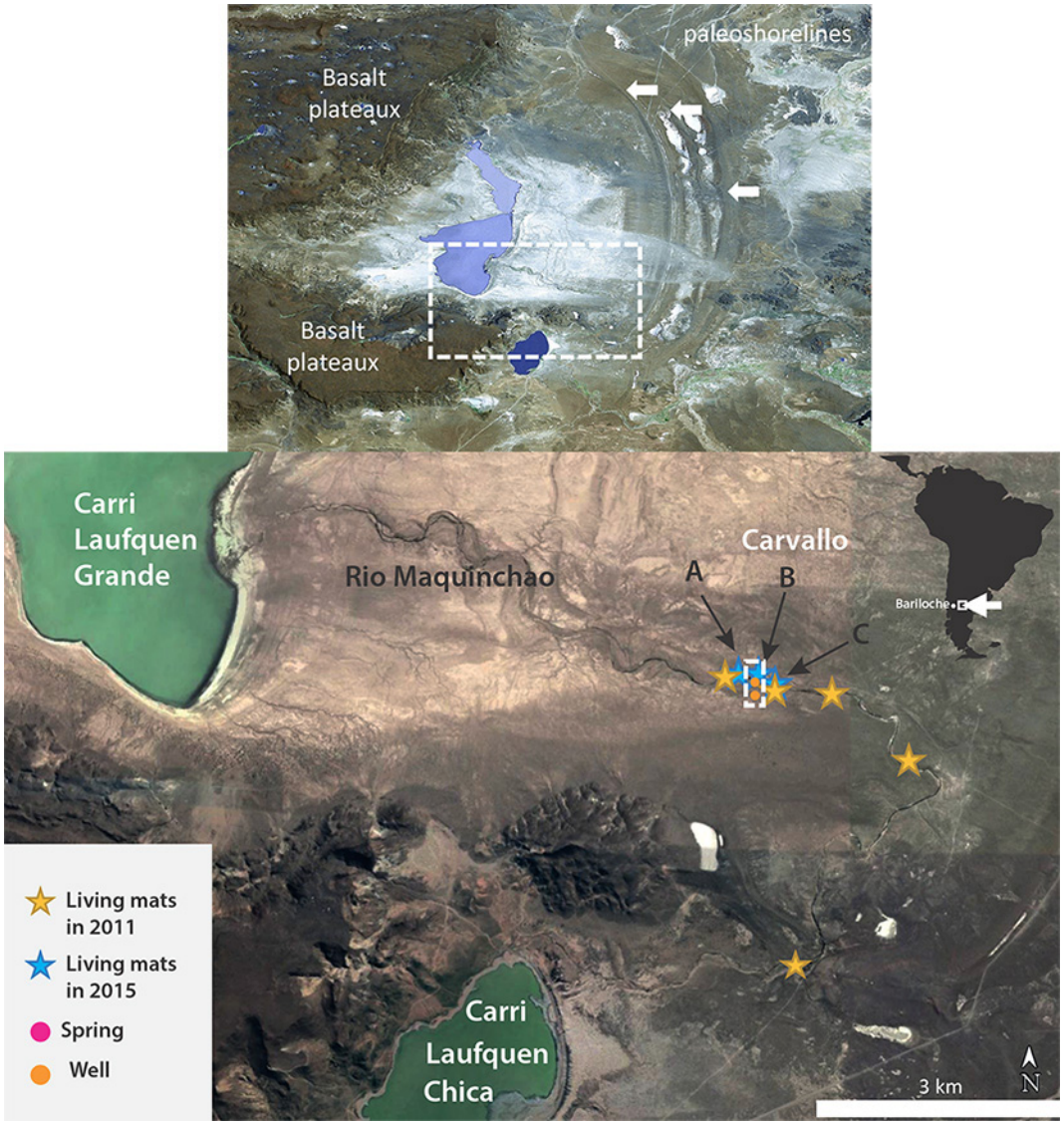

Figure 1. Satellite image of the Maquinchao Basin showing the location of both modern lakes Carri Laufquen Grande (CLG) and Carri Laufquen Chica (CLC), the Maquinchao River as well as the main basalt plateaux and the largest paleoshorelines (white arrows). Bottom panel displays sampling locations of microbial mats indicated as A, B and C whereas dashed white rectangle indicates water sampling locations.

isolated using PVC tubes and closed securely to avoid sediment incorporation. In total five sampling places were defined, including two lake surface waters, one river surface waters, and two pits waters (Fig. 1; Alvarez *et al.*, 2021). Chemical analyses of waters have been performed in the *Laboratorio de Suelos de Ecosistemas Patagónicos*, from the *Instituto Patagónico para el Estudio de los Ecosistemas Continentales* and in the *Laboratorio de Geoquímica del Centro de investigaciones Geológicas*, Argentina. Carbonates, bicarbonates, chlorine, calcium and magnesium have been measured by titration. Sodium, and potassium by photometry and sulfates by UV spectrophotometry. Chemical analyzes were processed and Saturation Indexes (SI) calculated using the software DIAGRAM and PHREEQC, respectively.

Mats sampling and SEM preparation

Mats were sampled during Austral spring 2015 in three different locations A, B and C (Figs. 1 and 3). In location A, the system is composed of several small streams of few centimeter depth (up to 10cm) running west towards CLG. Location B and C are slightly deeper (up to 50cm). Waters are

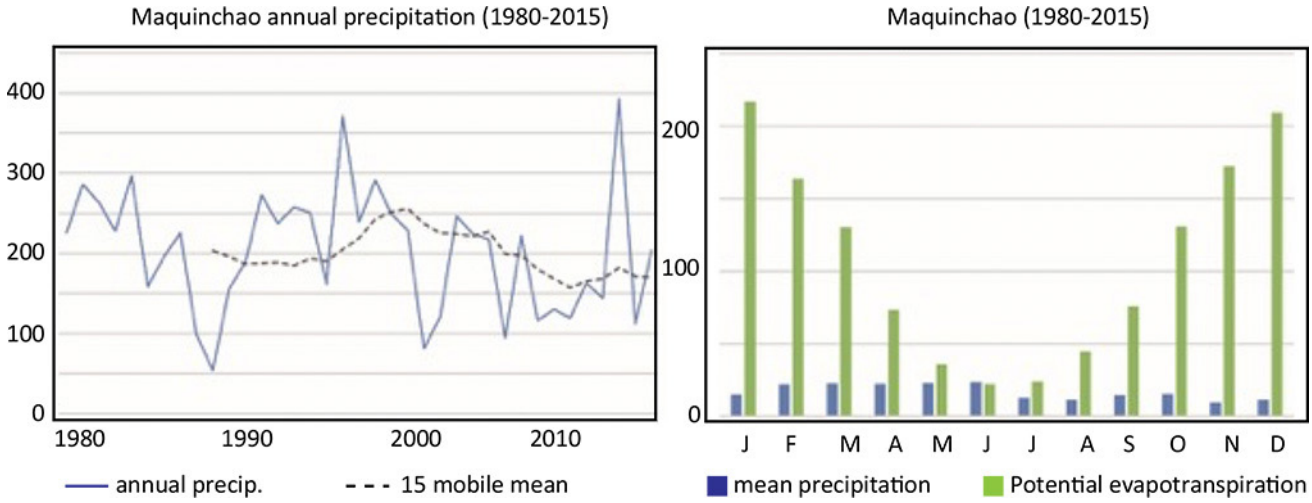

Figure 2. Annual precipitation (in mm) in the Maquinchao Basin from 1980 to 2015 (left). The bar chart on the right displays the average precipitation (blue) in mm per month for the same time interval compared to the corresponding potential evapotranspiration (green).

very still, and flow runs toward west in direction to CLG. All samples were fixed in the field using Glutaraldehyde (2.5%). A sample from location A was retrieved in the center of the stream/channel whereas in location B was taken from the top part of a large pebble and both samples were directly put in tubes with Glutaraldehyde. Samples from location C were carried and stored in a larger container for several days before being fixed with glutaraldehyde. All samples were subsequently dehydrated with increasing ethanol concentrations (30%, 50%, 70%, 90%). Back in the laboratory they were either directly mounted on stubs and gold coated for SEM observations or dehydrated using a critical point device. When possible, samples were mounted to allow the observation of both their upper and bottom sides as well as a longitudinal section.

Mats observations and the identification of elemental phases were performed by Scanning Electronic Microscopy (SEM) and Energy Dispersive Spectroscopy (EDS), respectively. The SEM-EDS analyses were carried out using a JEOL 7001 PA Scanning Electronic Microscopy instrument, equipped with an Energy dispersive X-ray analyzer EDS JED2300 at the Department of Earth sciences of the University of Geneva (Switzerland).

Molecular Biology

Samples for microbiological/DNA sequencing study were collected in several pounds (Fig. 1) using sterilized scalpels. All samples were stored in tubes (with ethanol) and kept refrigerated until further processing. Samples from locations A, B and C were divided in three subsamples: the top (1), the center (2) and the lower part (3). In location A, the sample was taken from the border and the center of the channel/stream. A1 and A2 correspond to samples taken from the rim having a jelly texture and being drier, respectively. A3 has retrieved from the center of the stream/channel.

DNA extraction was performed in 0.5 mg of processed sample using the kits MOBIO POWER BIOFILM. DNA amplifications were conducted with a total of ~10 ng of DNA using universal Primers for prokaryotes Pro341F (SEQUENCE 5'-CCTACGGGNBGCASCAG-3') and Pro805R (5'-GACTACNVGGGTATCTAATCC-3') for the V4-V5 hypervariable region of 16S rRNA gene (Takahashi *et al.*, 2014). Polymerase Chain Reaction (PCR) Products were then purified with Kit Roche HighPure PCR Protocols beads (Roche) and triplicates were quantified and pooled. Samples were then pooled equimolarly and Qubit-quantified for DNA sequencing.

Sequencing was performed at the University of Geneva (Switzerland), on an Illumina Miseq with 2x250 cycles with settings of 7.5 GB yield (including PhiX), an error rate of 2.5% and Q30 at 75%. The analysis yielded 5.3GB of sequence with an error rate within quality specifications. After barcode and primer trimming were removed using the in-house

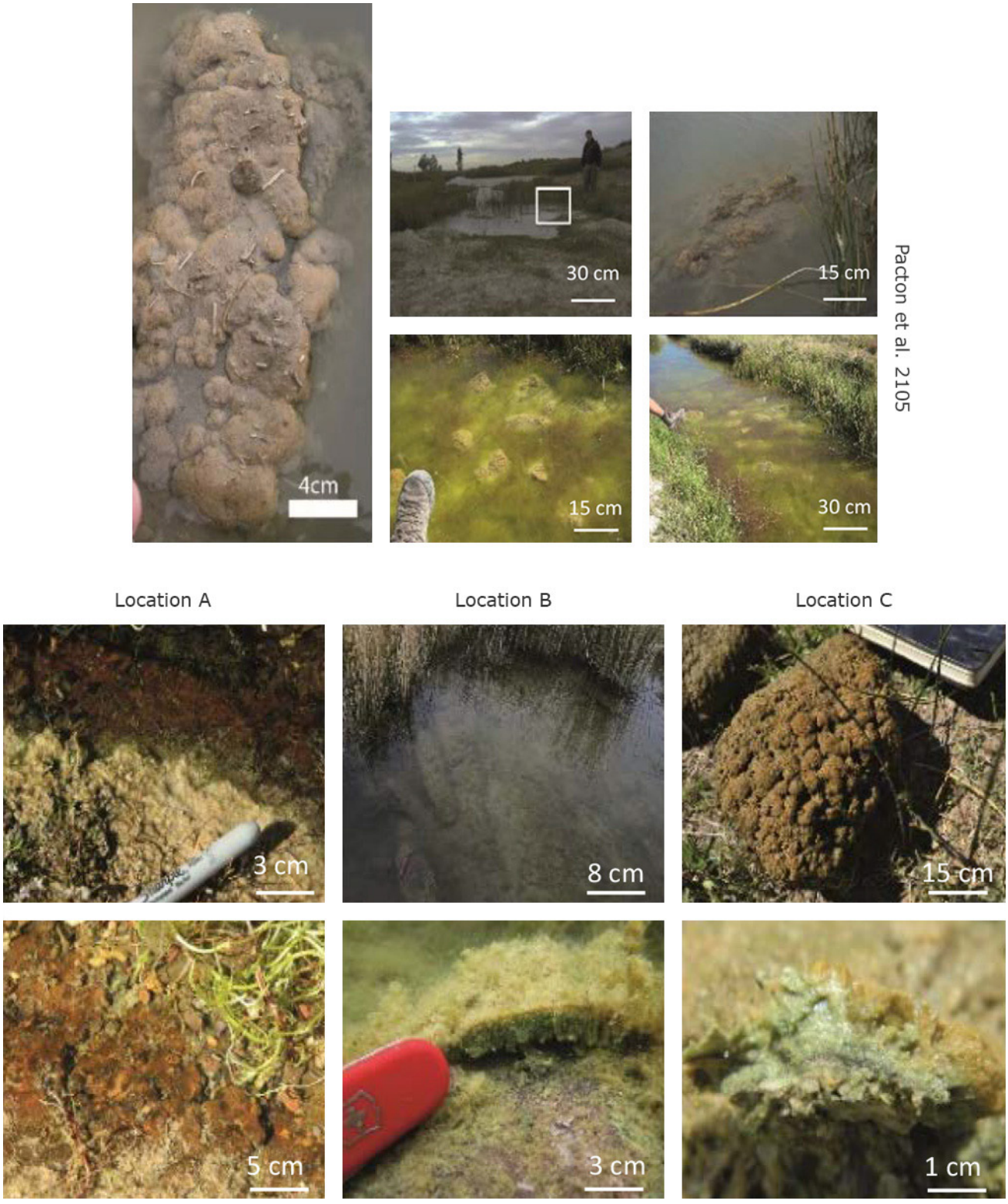

Figure 3. Panel I (top): Modified field photographs of microbial mats observed in 2011 by Pacton *et al.* (2015). Panel II (bottom): Photographs of the river/pond and microbial mats in 2015 for each mat sampling site. Refer to Figure 1 for location of sampling stations.

script, sequences were quality controlled, denoised, paired-ends merged and chimeras were removed using DADA2 version 1.20.0 (Callahan *et al.*, 2016) using R. Sequences were then classified as amplicon sequence variants (ASVs). These ASVs were taxonomically assigned using Silva (138.1 release)

(Quast *et al.*, 2013) and figures and data obtained using the phyloseq package after rarefaction to 90% of the least abundant taxa in a sample (McMurdie and Holmes, 2013). R scripts are available on the following links : https://osf.io/ngpce/.

RESULTS AND DISCUSSION

Water chemistry

Waters in the Maquinchao Basin can be divided in three different groups according to their sampling location: (1) CLGs; (2) CLCs; and (3) Carvallo Maquinchao CLA 2P and CLA 3P. A more detailed discussion of these data can be found in Alvarez *et al.* (2021). The collective water sampling campaigns allowed to have a water dataset for the different seasons. This is clearly noticeable in the temperature dataset, where the lowest temperatures are registered during the Austral winter (Table 1). Conversely, temperatures appear to remain relatively uniform between surface water in the river and water from the pits regardless of the season. The pH values range from 7.2 to 9.9 being the highest associated with the present lakes. The river values are slightly higher than the one from the pits no matter the season. Conductivity in CLG displays the highest values ranging from 10100 to 631000 μS/cm.

Major elements display differences between the lakes and the river and changes between the different sampling campaigns can be identified. Waters cations abundance are as follow: $Na^+ >> Mg^{2+} > Ca^{2+} > K^+$ (Table 1). Na^+ values are the highest by far in CLG ranging from 117 meq/L in February 2017 to 626.1 in November 2015. In comparison, Na^+ values for CLC river and pits are lower, ranging from 4.2 meq/L to 24 meq/L. Most of Na^+ values in river and pits are constant throughout seasons and years and are around 10 to 12 meq/L. Concentrations in major elements remain generally constant in river point and its associated pits. The same trend of higher values in CLG compared to CLC, river and their associated pits can be observed for K^+ and Mg^{2+}. In comparison, Ca^{2+} presents a different trend. Firstly, Ca^{2+} concentrations in CLG are lower (0.2 to 0.6 meq/L) than the ones from CLC, river points and their associated pits. Carvallo river values are homogenous along the different campaigns (from 1.7 to 2 meq/L) whereas values for the associated pits fluctuated during the different sampling seasons. Cl^-, SO_4^{2-} and Na^+ present similar variation trends. In addition, sulfates values appear to be higher in pits than in their associated river points. As for anions, CO_3^- was quasi absent, and only recorded in CLG (0.9 to 17.1 meq/L). Conversely, bicarbonates (HCO_3^-) showed substantial variations. CLG values are lower during summer periods than during autumn and winter seasons. Furthermore, during these last two seasons differences between river and associated pits are less marked than during summer and spring. Fluctuations of Ca^{2+} are lower than the ones of HCO_3^-. River waters present less variations in all ions than its associated pits (Fig. 4). All ion values during Austral spring 2015 are lower especially for CLC compared to the values for the other periods and years (Table 1; Fig. 4). This is especially obvious for HCO_3^- (Fig. 4)

Saturation Indexes (SI) of different minerals have been calculated for all sampling points and field campaigns. SI for anhydrite, gypsum and halite delivered numbers below 0 thus proving the undersaturation of the waters in the Maquinchao Basin (Table 2). $SI_{calcite}$ values range from -0.98 to 1.22, indicating undersaturated to saturated waters for calcite. Both CLG and CLC present strong variations of the SI with period of $SI > 1$ and $SI < 0$ (Table 2, Fig. 4). In comparison, SI from river point and its associated pits are always below 1 and usually below 0.8 SI. River SI values are higher than the ones from its related pits. Winter and autumn SI for river points and its connected pits are higher than SI for spring and summer.

This dataset indicates that the November 2015 values have different ranges compared to the other campaigns and are slightly lower. There are two different trends, one for lakes and one for the river that are consistent with Pacton *et al.* (2015) observations. Variations in both lakes can be strong whereas the river data are more homogenous and stable.

Mats diversity and morphologies

Three different mats have been sampled during the 2015 field campaign in locations A, B and C (Figs. 1 and 3). The sampling site A had a hard substrate and was located in shallow waters. The site B was located in a large pound protected by vegetation that does not dry out (pers. comm. from locals). Monitoring of waters has been carried out in

Date	Season	Sample	Descriptif	CD (uS/cm)	PH	T°	O_2 (mg/l)	Na meq/l	K meq/l	Ca meq/l	Mg meq/l	CO_3 meq/l	CO_3H meq/l	meq SO4/l	Cl meq/l
November 2015	Austral Spring	CLG-1S	CLG surface	63100.0	9.4	14.3	8.3	626.1	7.2	0.2	37.4	0.9	1.3	428.1	397.2
November 2015	Austral Spring	CLC-1S	CLC surface	865.0	9.2	19.0	9.1	4.3	0.3	1.9	2.8	0.0	2.6	2.8	1.6
November 2015	Austral Spring	Aª Carvallo	River Carvallo	1309.0	7.9	20.0	9.1	7.8	0.3	1.9	2.8	0.3	2.5	5.4	3.1
November 2015	Austral Spring	CLA-2P	Well	1644.0	8.0	17.0	9.4	12.3	0.4	1.8	1.9	0.0	4.0	7.3	4.7
November 2015	Austral Spring	CLA-3P	Well	1461.0	7.8	16.0	9.5	10.2	0.2	2.0	2.1	0.0	4.3	6.1	3.4
April - May 2016	Austral Autumn	CLG1S	CLG surface	32400.0	9.8	s/d	8.9	260.9	10.7	0.3	12.4	14.4	37.0	72.9	230.7
April - May 2016	Austral Autumn	CLC1s	CLC surface	1220.0	9.4	s/d	8.5	7.4	0.3	2.7	2.7	0.0	6.6	5.9	3.0
April - May 2016	Austral Autumn	Aª Carvallo	River Carvallo	1359.0	8.2	s/d	8.9	11.7	0.5	2.1	2.7	0.0	6.6	3.1	3.1
April - May 2016	Austral Autumn	CLA2p	Well	1308.0	8.0	s/d	8.6	13.7	0.2	1.9	1.7	0.0	8.3	3.6	2.9
April - May 2016	Austral Autumn	CLA3p (3-1)	Well	1316.0	7.3	s/d	8.7	12.6	0.2	2.1	2.4	0.0	8.1	3.1	2.8
August 2016	Austral Winter	CLG1S	CLG surface	32900.0	9.9	s/d	9.7	360.9	7.2	0.2	8.8	17.1	16.3	255.0	189.4
August 2016	Austral Winter	CLC1S	CLC surface	11190.0	7.4	4.9	9.2	6.3	0.3	1.6	2.6	0.0	6.9	2.6	2.5
August 2016	Austral Winter	Aª Carvallo	River Carvallo	1425.0	7.9	s/d	9.7	11.7	0.3	1.8	2.8	0.0	7.2	3.5	3.7
August 2016	Austral Winter	CLA2P	Well	1325.0	7.9	9.3	9.2	12.0	0.2	1.4	1.4	0.0	7.8	2.5	3.4
August 2016	Austral Winter	CLA3P	Well	2231.0	7.5	5.9	9.2	24.3	0.6	2.8	3.9	0.0	13.6	6.1	6.4
February 2017	Austral Summer	CLGs	CLG surface	10100.0	9.9	23.7	6.5	117.4	6.9	0.6	2.5	7.2	5.3	25.0	67.7
February 2017	Austral Summer	CLCs	CLC surface	1289.0	9.2	15.5	6.6	11.1	0.6	1.3	3.6	0.0	7.8	4.4	2.8
February 2017	Austral Summer	Aª Carvallo	River Carvallo	1272.0	7.9	17.7	8.6	10.4	0.4	2.0	3.0	0.0	6.5	5.5	2.9
February 2017	Austral Summer	CLA 2P	Well	1258.0	7.9	16.6	7.0	12.4	0.5	1.0	1.4	0.0	7.1	3.4	2.7
February 2017	Austral Summer	CLA 3P	Well	1537.0	7.4	17.0	8.6	15.0	0.5	2.0	2.2	0.0	9.0	3.5	3.4
March 2018	Austral Summer	CLCs	CLC surface	1175	9.13	15.7	s/d	8.2	0.6	1.2	3.8	1.6	4.5	1.3	2.8
March 2018	Austral Summer	Aª Carvallo	River Carvallo	1170	7.82	12.2	s/d	9.0	0.4	1.7	3.4	0.0	5.8	3.9	2.9
March 2018	Austral Summer	CLA2P	Well	1077	8.1	15	s/d	11.3	0.4	0.4	2.2	0.0	6.4	4.3	2.2
March 2018	Austral Summer	CLA3P	Well	1242	7.32	16.8	s/d	12.2	0.4	2.0	2.2	0.0	7.6	3.9	2.7

Table 1. Physicochemical parameters of water samples.

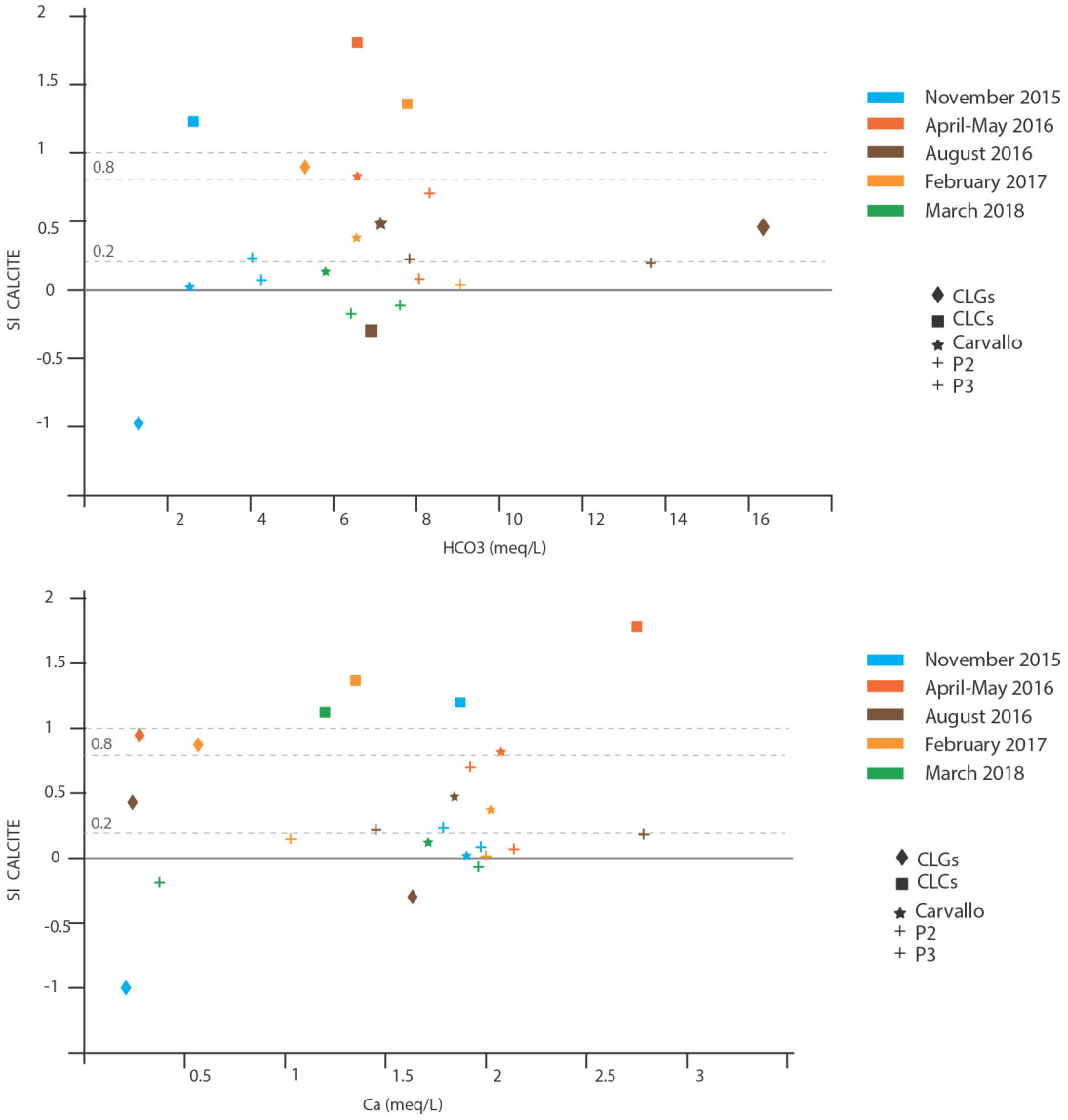

Figure 4. Saturation Index for calcite vs. HCO_3^- (uppermost panel) and Ca (lowermost panel). Colors indicate different sampling periods whereas symbols stand for sampling locations.

sampling site B at the exact site where mats have been sampled (water sampling point named Carvallo, see Fig. 1). Location C was set in a larger pound affected by water level variations.

The uppermost part of the mat from location A is reddish presenting black spheres also known as Nostoc balls (Dodds *et al.*, 1995). It also contains abundant diatoms decreasing with depth. Three different types of filament assemblages can be distinguished under SEM (Fig. 5). Certain areas are characterized by abundant filaments of variable diameter having an outer sheath (Fig. 5a to g). They can be associated with dense calcium carbonate forming molds around the filaments (Fig. 5a); not embedded but having small crystals forming on top of them; or not associated at all with calcium carbonate (Fig. 5b). In the first case most of the time only the outer sheath is preserved (Fig. 5c). Furthermore, the OM structure is still visible as a very thin matrix in the molds, and all-around molds area (Fig. 5d, e, f). On the other hand, some areas display more diversified microbial morphologies (Fig. 5g, h, i), presenting filaments of different diameter but mostly thinner than in the areas of dense filaments (Fig. 5g), as well as coccoids (Fig. 5h, i), bacilli-like (Fig. 5j) and stacks of rounded microorganisms (Fig. 5h). A very fine matrix is also present (Fig. 5i) that in certain areas is associated with small thin minerals (Fig. 5j). The

Date	Season	Sample	Descriptif	SI calcite	SI gypsum	SI anhydrite	SI halite
November 2015	Austral Spring	CLG-1S	CLG surface	-0.98	-1.9	-2.13	-2.52
November 2015	Austral Spring	CLC-1S	CLC surface	1.22	-1.83	-2.07	-6.84
November 2015	Austral Spring	Aª Carvallo	River Carvallo	0.02	-1.57	-1.81	-6.29
November 2015	Austral Spring	CLA-2P	Well	0.23	-1.51	-1.76	-5.93
November 2015	Austral Spring	CLA-3P	Well	0.06	-1.51	-1.76	-6.14
April - May 2016	Austral Autumn	CLG1S	CLG surface	0.95	-2.34	-2.55	-3.13
April - May 2016	Austral Autumn	CLC1s	CLC surface	1.8	-1.53	-1.75	-6.36
April - May 2016	Austral Autumn	Aª Carvallo	River Carvallo	0.82	-1.81	-2.03	-6.13
April - May 2016	Austral Autumn	CLA2p	Well	0.7	-1.78	-2	-6.11
April - May 2016	Austral Autumn	CLA3p (3-1)	Well	0.07	-1.78	-2	-6.15
August 2016	Austral Winter	CLG1S	CLG surface	0.45	-1.97	-2.18	-3.11
August 2016	Austral Winter	CLC1S	CLC surface	-0.3	-1.86	-2.12	-6.44
August 2016	Austral Winter	Aª Carvallo	River Carvallo	0.48	-1.81	-2.03	-6.07
August 2016	Austral Winter	CLA2P	Well	0.22	-1.96	-2.22	-6.04
August 2016	Austral Winter	CLA3P	Well	0.18	-1.47	-1.72	-5.49
February 2017	Austral Summer	CLGs	CLG surface	0.89	-2.02	-2.25	-3.92
February 2017	Austral Summer	CLCs	CLC surface	1.35	-1.9	-2.15	-6.18
February 2017	Austral Summer	Aª Carvallo	River Carvallo	0.37	-1.57	-1.81	-6.21
February 2017	Austral Summer	CLA 2P	Well	0.15	-2.01	-2.26	-6.16
February 2017	Austral Summer	CLA 3P	Well	0.02	-1.76	-2.01	-5.99
March 2018	Austral Summer	CLCs	CLC surface	1.13	-2.37	-2.62	-6.31
March 2018	Austral Summer	Aª Carvallo	River Carvallo	0.13	-1.74	-2	-6.25
March 2018	Austral Summer	CLA2P	Well	-0.18	-2.36	-2.61	-6.27
March 2018	Austral Summer	CLA3P	Well	-0.12	-1.7	-1.95	-6.17

Table 2. Variations in saturation indexes (SI) for calcite, gypsum, anhydrite and halite for different sites and seasons of the year.

abundance of microorganisms decreases as calcium carbonate increases, forming clusters of very small crystals. The mineral and OM fractions appear to be tightly linked (Fig. 5k), some areas present an alveolar structure made up of an organic sheath and calcium carbonate (Fig. 5l). Calcite is visible above the sheath as a stack of platelet of rhombohedral crystals (Fig. 5m). Rounded structures of possibly microorganisms can be observed under the sheath (Fig. 4n), and in some areas of crack sheath calcium carbonate precipitates are visible (Fig. 5o).

The sample of location B presents diatoms on the top part of the mat. It is composed of filaments of different diameters, abundant bacilli and a very thin organic matrix (Fig. 6a, b). Below, the mat is still composed of abundant bacilli of different sizes, as well as coccoid, diatoms and to a lesser extent filament remains (Fig. 6c, d). A thin, calcium-rich organic matrix is also visible everywhere and in many areas its density creates an OM film (Fig. 6d, e). This calcium-rich phase associated with calcium carbonate minerals is observed below the film and associated with a Mg-Si phase (Fig. 6e).

The mats in location C are similar to location B since both areas display comparatively higher water depths and present a low-to-no energy environment. In both locations microbial mats were attached to basalt pebbles and presented an uppermost yellowish

part, the rest of the mat being greenish (Fig. 3). SEM inspection shows areas of filaments associated with clusters of calcium carbonate minerals (Fig. 7a, b) for location B. Other parts are highly mineralized with platelet and arrow shape calcium carbonate associated with OM film (Fig. 7c, d). Some areas present rounded forms underneath the organic film and abundant diatoms (Fig. 7e, f). Finally, certain zones present a very thin organic matrix associated with calcium carbonate precipitate and a Si phase (Fig. 7g, h, i). EDS analyses indicate the presence of Ca and recurrent Mg, Al and Si phases. The mat in location B is less mineralized in comparison to the samples from sites A and C (Fig. 6). Filaments, however, are recurrent in all three samples.

Analysis of microbial communities based on 16S rRNA gene sequences

The sequencing using the 16SrRNA of the mats provides information on the prokaryote communities present in the samples. Three samples ca. 1mm thick have been taken from the three different mats. Samples from location B and C without clear laminas were sampled at the surface, 3 to 4 mm depth and 6 to 8 mm depth seeking for possible differences in communities between uppermost, center and lower parts of the mats, respectively. Pacton *et al.* (2015) described the presence of an upper layer of filamentous and coccoid *Cyanobacteria* associated with a carbonate phase whereas the lower layer contained abundant SRB and substantially higher content of carbonate. Hence, we have focused the analyses of the results of 16S rRNA mainly on those two groups. *Cyanobacteria* were hardly detected in the 16S rRNA gene sequences (only a few ASVs, all lost after rarefaction was applied). This being said, microscopic observations attest of the presence of photosynthetic organisms, including diatoms and green-pigmented filaments. It is however clear that phototrophic prokaryotes did not account for an important fraction of the 16S rRNA gene libraries obtained (Fig. 8). As an example, only 3 ASVs affiliated to *Chloroflexi* were obtained after rarefaction to 2370 taxa per sample.

Desulforbacterota (mainly composed of sulfate reducing organisms; Waite *et al.*, 2020) are much more common, ranging between 14 % (maximum in A3, bottom of mat from zone A) and 0.8 % (minimum in C3, bottom from zone C) (Fig. 9). They are represented in the samples as *Desulfobulbia* occurring in all samples, *Desulfovibrionia* and *Desulfobacteria* (Fig. 9). *Desulfurmonada* sequences were also obtained, but in lower read abundance (Fig. 9). No clear distinction could be made based on site or microbial mat zone (top/center/bottom), in line with the limited stratification observed for each mat.

Implication of physico-chemical extrinsic parameters in carbonate precipitation

A difference in water chemistry is obvious between the lakes and the river sampling sites. The lakes present greater fluctuations in chemistry especially CLC, but overall, they tend to have sulfate-rich waters compared to the Maquinchao River, that presents rather bicarbonate-rich waters. Moreover, as the chemical data from the drilled wells are comparable to the river sampling point, it can be suggested that the lakes greater fluctuation in size is mostly related to the bi-water sources feeding it - underground and meteoric- and, thus highly dependent on rainfall (meteorological impact). Although no quantified in this study, evapotranspiration changes and high wind velocities might also impact the lake levels and their water chemistry. The Maquinchao River is more resilient due to the largest groundwater input compared to meteoric waters. Furthermore, although fluctuating over the monitored interval the $SI_{calcite}$ results show mostly slight saturation (~0.8) to saturation (~1.8) in both lakes. However, the mineralizing mats described in 2011 and microbial mats in general were only reported in some particular areas of the river. It is unlikely that the chemistry only would promote the growth of microbialite in the river rather than in the lakes. Nevertheless, calcium and bicarbonate are critical for the formation of microbialites (Farías *et al.*, 2013). The brackish to saline waters of both lakes could prevent microbial mats proliferation compared to the more freshwater river as proposed by Pacton *et al.* (2015). Additionally, changes in certain factors such as chemistry and water level, associated with turbidity of the water, would be concurrent and limiting factors for the development of microbial mats.

To precipitate calcium carbonate SI must be above 0. However, according to Merz-Preiß (2000), *Cyanobacteria* encrustation, also known

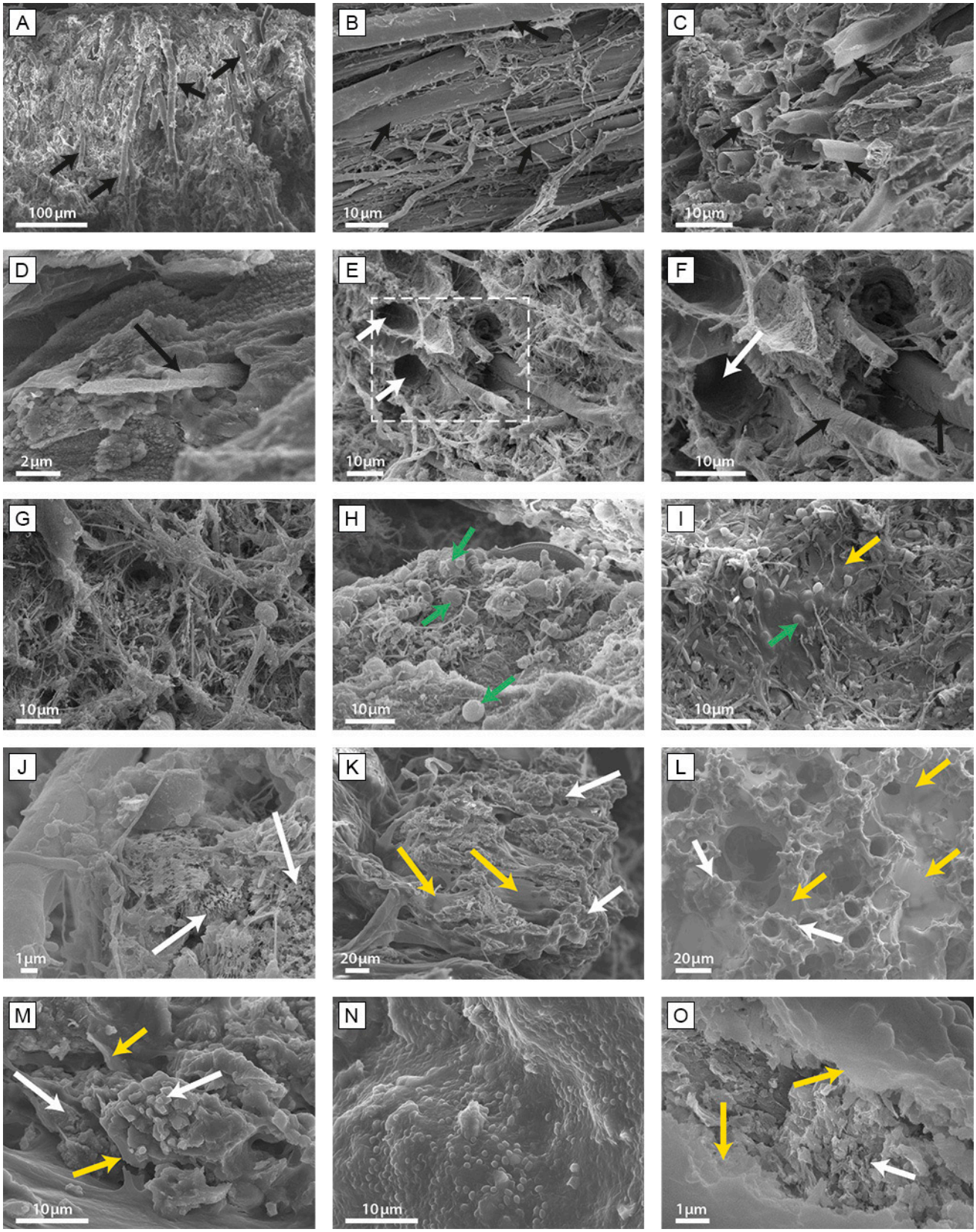

Figure 5. SEM photomicrographs of samples from location A. Panels A, B, C, D, E and F correspond to samples that have been taken from the center of the stream/channel. Panels G, H, I, J, K, L, M, N, O are from samples that have been taken towards the side of the stream/channel. **a)** Erect filaments (black arrows) associated with carbonate precipitation. **b)** Filaments (black arrows) of various widths. **c)** Preserved outer sheaths (black arrows) encrusted in carbonates. **d)** Fully preserved encrusted filaments (black arrow) under higher magnification. Sheath appearance suggests mineralization. Organic thin sheath can be

as *biologically-influenced* mineralization, happens for SI > 0.8 in the water. SI < 0.8 would lead to more biologically induced processes involved in carbonates formation. Both lakes happen to present values above 0.8 but do not show carbonate precipitation. The absence of microbial mats in both lakes probably prevent the precipitation of carbonates as microbial mats often play the role of preferential nucleation sites (Riding, 2011a). In contrast, Maquinchao River SI have been barely reaching 0.8 during the different sampling periods, suggesting that organomineralization would mainly be the result of biologically-induced processes (Merz-Preiß, 2000).

In 2015, however, the mineralization of the mats, at least in location B and C, was low. Lower values for major elements and especially bicarbonate have been recorded, thus affecting, and giving lower SIcalcite in 2015 compared to the subsequent sampling seasons (Fig. 4, tables 1 and 2). The already arid character of the climate in the Maquinchao area has been harden due to a decrease in rainfall from years 2000 to 2011 affecting the lake levels and river as well as the aquifers. However, the years 2014 and 2015 have had comparatively higher rainfall (380mm in 2014; Fig. 2). This meteoric source could have substantially lowered the concentration of major elements in the Maquinchao River. Meteoric waters are less rich in cations and anions, including Ca^{2+} and HCO_3^-, in comparison to underground waters, which would have been enriched by the dissolution of the rock reservoir. Meteoric waters would have overtaken underground inputs leading to lower SI in 2015 and consequently diminishing carbonate mineralization. Physico-chemical data between 2011 and 2015 and onward have substantially changed, making their comparison difficult (tables 1 and 2). However, in the light of the chemical information, pH and Ca^{2+} seem to be more or less stable over the years and seasons except in 2015. Furthermore, the increasing amount of calcium carbonate minerals in the lower part of the mats in 2011 would be in favor of a low $SI_{calcite}$ as otherwise mats would tend to be more mineralized especially on the upper green part that would serve as a substrate site for abiotic calcium carbonate mineralization. The increasing alkalinity in the lower part of the mat lead to carbonate precipitation by the metabolic action of microorganisms (Pacton *et al.*, 2015). However, in 2014-2015 even if microbial activity could substantially increase the alkalinity and pH within the mat, the depravation in bicarbonate in the environment and calcium in the Maquinchao River due to the increased meteoric contribution compared to groundwater inputs might have decreased the precipitation of $CaCO_3$ in the mat. An additional factor that cannot be neglected is the Puyehue 2011 and Calbuco 2015 volcanic eruptions that had a strong impact in the region and might explain the lack of organomineralization in 2015 compared to what had been observed in 2011.

Sampling location A presents much more mineralization than locations B and C. This mineralization is largely associated with filamentous organisms. Calcium carbonate precipitation associated with filamentous cyanobacteria has been largely described in many sites (Freytet and Verrecchia, 1998; Merz-Preiß, 2000; Roche *et al.*, 2019). Furthermore, the presence of a stream in sampling site A implies a higher energy environment compared to locations B and C. Physical degassing of CO_2 may occur in streams/fast flowing waters. This phenomenon is one of the potential external parameters involved in carbonate precipitation in lacustrine microbialites (Dupraz *et al.*, 2009). The presence of flowing water and carbonate formation

observed below the filament. **e)** View of the remaining tubular molds (white arrows). **f)** Enlargement (dashed-line rectangle in d) of the remaining tubular molds (white arrows). Preserved sheaths can be observed in between (black arrows). Organic sheath associated with the molds. **g)** Highly diversified microorganisms including filaments of different length and width, coccoids and bacillis. **h)** Area rich in coccoid bacteria (light green arrows). **i)** Microorganisms (light green arrows) below an organic sheath. **j)** Very small minerals precipitates interconnected by very thin organic strands (white arrows). Coccoid and bacilli microorganisms are observed in the same area. **k)** Thin organic film (orange arrows) interconnected with mineral precipitates (white arrows). **l)** Ovoid pores presenting mineralized trim (white arrows) and interconnected by a thin organic film (orange arrows). **m)** Enlargement showing the interconnection between carbonate precipitates (white arrows) and organic film (orange arrows). **n)** Organic film covering areas presenting apparent rounded microorganisms. **o)** Enlargement of the area of the rectangle in N, revealing the presence of patched of small minerals (white arrow) under the thin organic film (orange arrows).

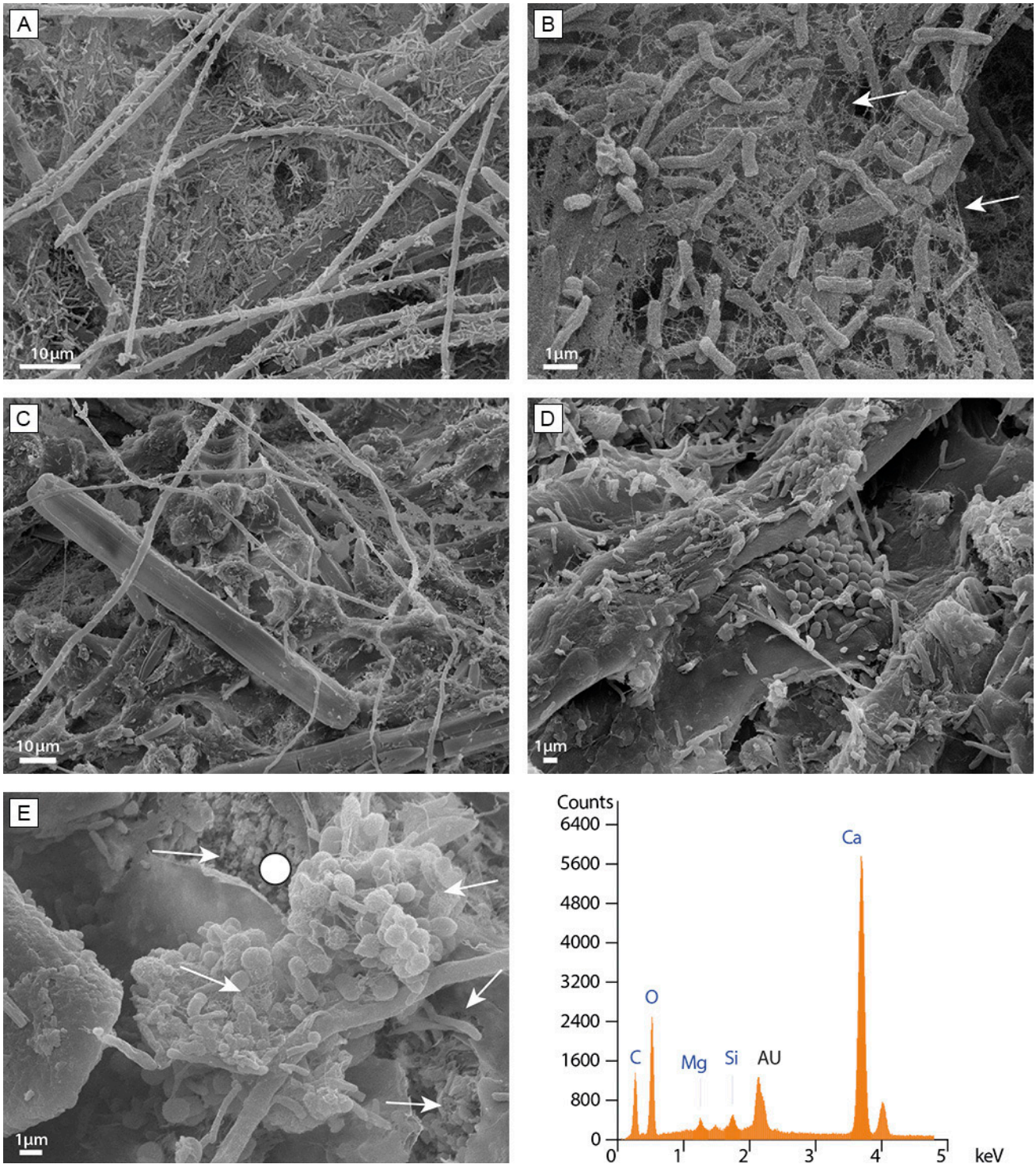

Figure 6. SEM photomicrographs and EDS analyses of sample from location B. **a)** Densely populated area composed of large filaments, thinner filaments and smaller bacteria attached either to the filaments or on the surface of an extensive organic matrix made of very thin strands. **b)** Enlargement of A, showing the organic matrix (white arrows) associated with the bacteria. **c)** Area displaying thin filaments and diatoms. **d)** Dense organic film mostly associated with coccoid than ovoid microorganisms. **e)** Photomicrograph showing clusters of bacteria (white arrows) behind an organic thin film. White dot indicates the location of EDS analysis showing a Ca-rich mineralization (bottom right).

around the filaments at location A (Fig. 5) favors a substantial abiotic impact in carbonate precipitation. However, biological uptake of CO_2 is also possible and should not be neglected. Photosynthesis is

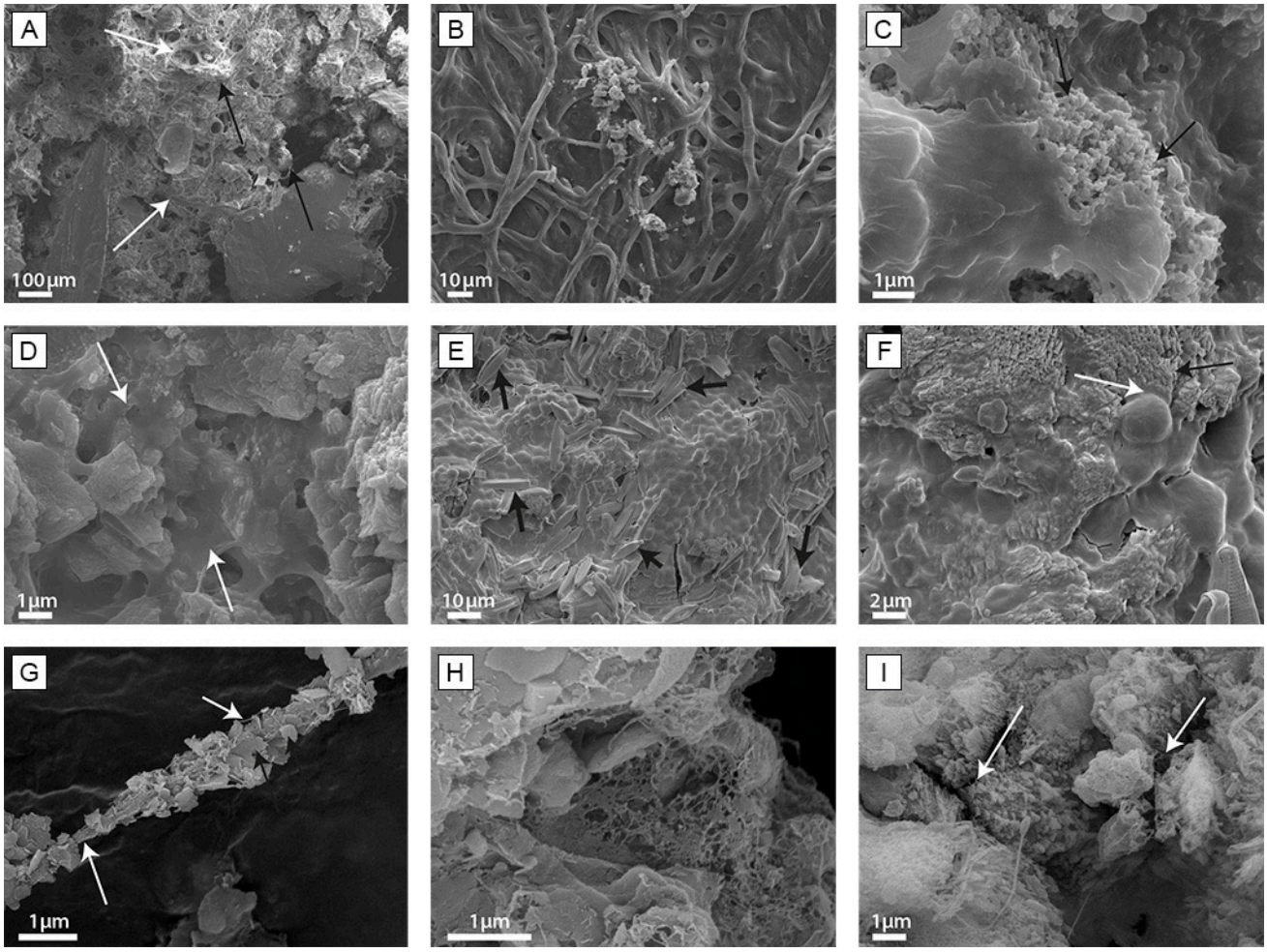

Figure 7. SEM photomicrographs of sample from location C. **a)** Filamentous network (white arrows) with nodules of carbonate precipitates (black arrows). **b)** Enlargement of the dense organic filamentous network. **c)** Small size crystals (black arrows) merging to form platelets. **d)** Platelets associated with a thin organic film (white arrows). **e)** Abundant diatoms (black arrows) observed on top of a thin organic film covering rounded cell shapes. **f)** Interconnection between the organic film (white arrow) and merging arrow-like precipitates (black arrow). Rounded morphologies of up to 2 μm can be observed under the organic film. **g)** Platelet minerals (black arrows) attached to thin organic string (white arrows). **h)** Dense organic strings. **i)** Nanometer carbonate minerals formed in association with thin organic strands (white arrows).

known to uptake CO_2 and increase alkalinity leading to favorable conditions for carbonate precipitation (Dupraz *et al.*, 2009). This can be achieved by Cyanobacteria and other primary producers such as diatoms. Here given the absence of 16S rRNA gene sequences associated to *Cyanobacteria*, we suspect the effect of *Cyanobacteria*, both for the production of alkalinity and EPS, to be minor. Nevertheless, the biofilm DNA extraction protocol, albeit adapted, may have negatively impacted cyanobacterial ASV relative abundance as these organisms are known for their protective sheath thickness. Additionally, diatoms can play a similar positive role in EPS and alkalinity production through photosynthesis, that cannot be neglected here (Figs. 6 and 7).

Potential microbial impact in carbonate precipitation

There are several differences between mats samples. Those from locations B and C are relatively similar encompassing a thin uppermost yellowish layer containing abundant diatoms that is overlying a greenish layer. In location A the uppermost layer is mostly reddish in color containing diatoms whereas the greenish layer is also thinner than in the previous locations. The structures observed in sample A differ from those described in Pacton *et*

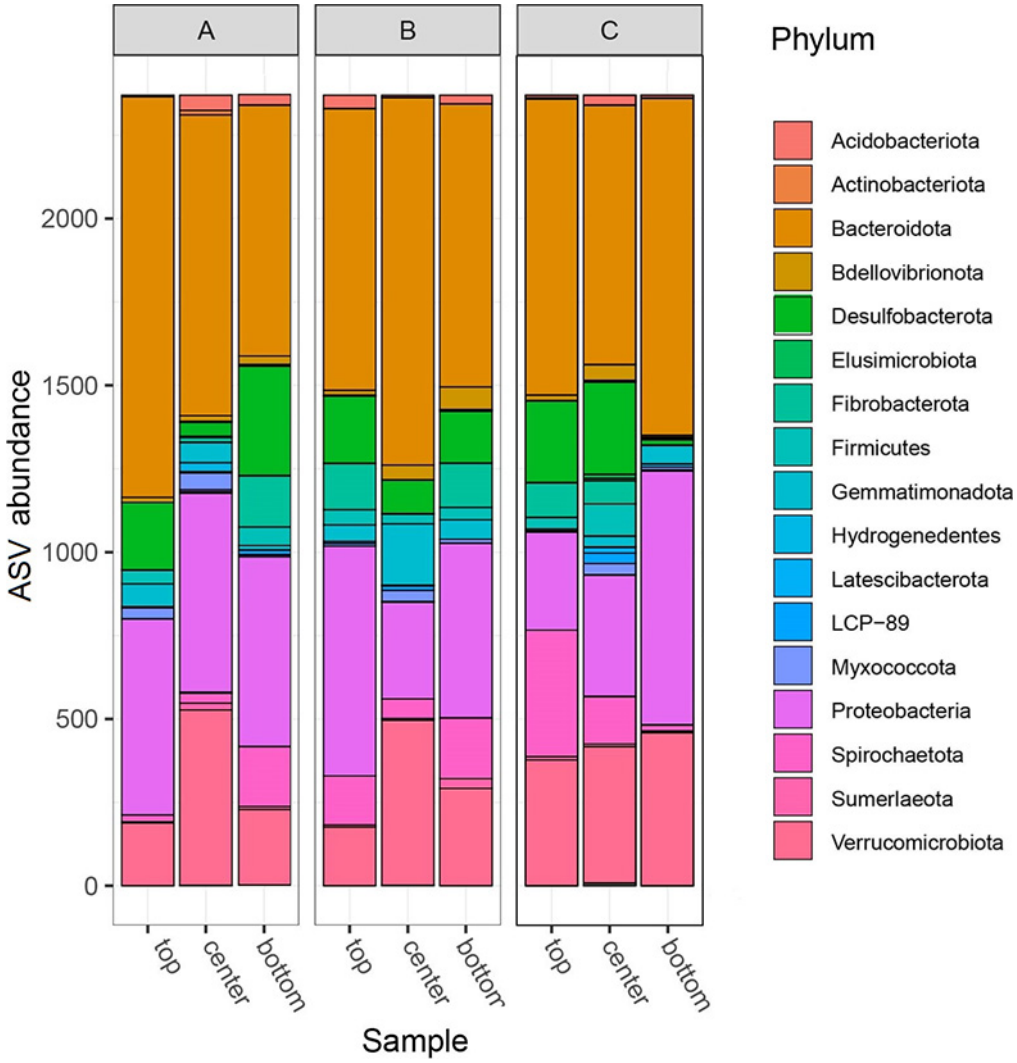

Figure 8. Bar chart of the abundances of rarefied ASVs affiliations at the phylum level in each sample for locations A, B and C.

al. (2015) that presented filamentous and coccoid *Cyanobacteria* as well as some SRB in the uppermost layer of the 2011 living mats containing few crystals of low Mg calcite. The beige layer in the lower part of the mat presented substantial $CaCO_3$ crystals associated with more abundant SRB.

At location B, no major mineralization has been observed neither associated with the large filaments, as described at location A, nor with other coccoids. The low $SI_{calcite}$ (<0.2) at the location of the sampling (Carvallo point) might have prevented the formation of $CaCO_3$ by extrinsic parameters. However, certain areas present small minerals as a matrix associated with OM remains (Fig. 6). The presence of this very restricted mineralization suggests a very localized alkalinity increase. EDS analyses of the mineralized area show a Mg-Si phase associated with the Ca signal. Mg-Si phases, if not detrital, have been reported in numerous environments and always related to microbial activity (Arp *et al.*, 2003; Souza-Egipsy *et al.*, 2005). These observations suggest that at location B intrinsic parameters (metabolic activity) may be involved in very moderate carbonate precipitation within the microbial mat. As the filaments are free of minerals and *Cyanobacteria* could not be detected in the genomic data (Fig. 8), heterotrophic microorganisms and in particular SRB (largely detected in our genomic data, Fig. 9) might be implicated, provoking a localized rise of alkalinity leading to carbonate precipitation and potential Mg-Si phase (Pace *et al.*, 2018). Locations B and C are both positioned in comparable environmental settings and an *in situ* macroscopic inspection of their microbial mats suggest that they are very

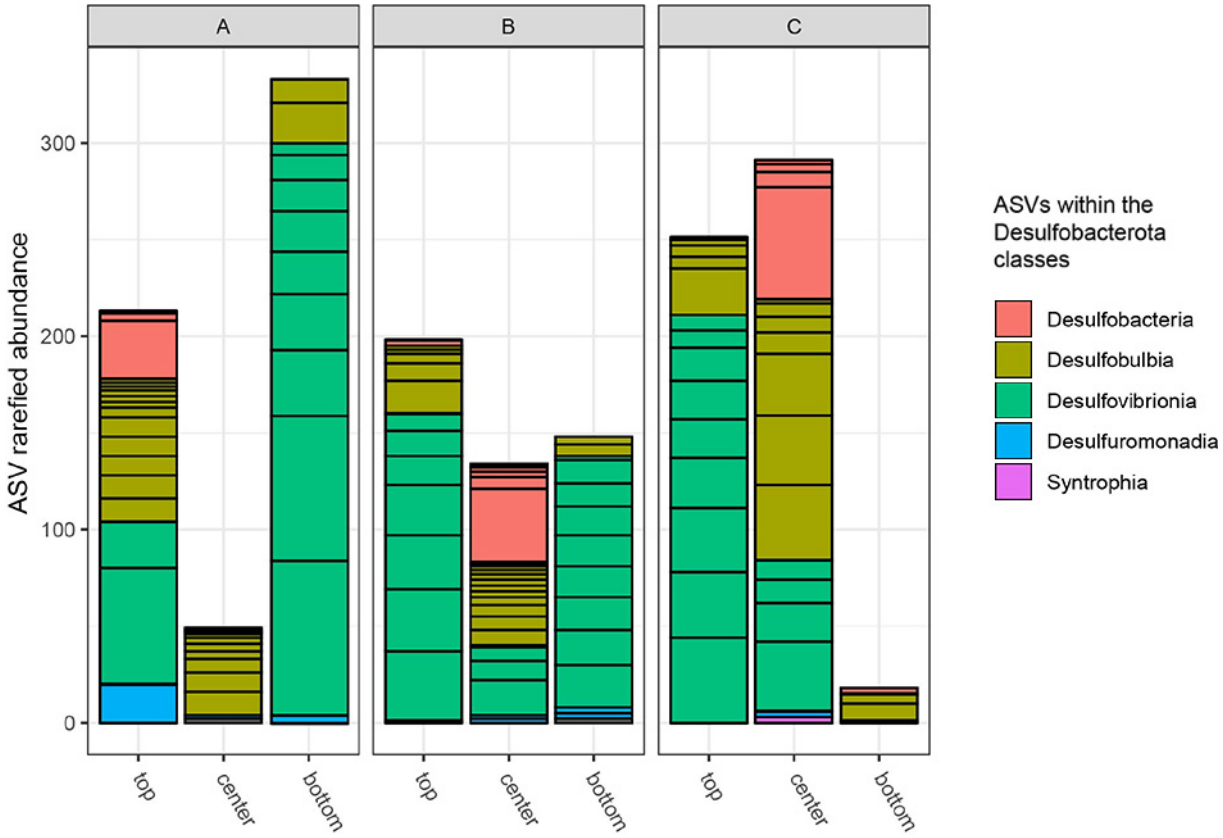

Figure 9. Barplot of rarefied Desulfobacterota ASVs at the class level, for each site A, B and C.

similar. They both display filaments although less abundant in location C than in B.

The sample from location A has different features than those from locations B and C. In sample A, the highly filamentous part associated with carbonates is very similar to what has been observed in dry crusts from the Maquinchao Basin. Molds of filaments are also observed (Fig. 5d-f). In many cases, an outer sheath is preserved that is often partially mineralized. Mineralization of filament sheaths has been described in various microbialites (Merz-Preiß, 2000; Wacey *et al.*, 2018; Gong *et al.*, 2019; Roche *et al.*, 2019). Filamentous molds preservation is often observed in systems where abiotic precipitation of carbonate is favored, thus, leading to the precipitation of carbonate on the surface of the microorganism/sheath and described as encrustation. Apart for incrustation, mineralization in the sheath may be also the result of carbonate impregnation (Merz-Preiß and Riding, 1999; Merz-Preiß, 2000; Riding, 2011b) produced by a rise of supersaturation within the film as a result of metabolic activity (Merz-Preiß, 2000) due to *Cyanobacteria* uptake of HCO_3^- for photosynthesis in waters of low pCO_2. In the studied mat of zone A, a dense carbonate matrix is visible in between filament molds suggesting encrustation (Fig. 5d-f). The presence of both types may suggest that even if extrinsic parameters play a role in carbonate precipitation, metabolic processes may have a very localized impact. These processes might have a changeable impact over time switching mineral precipitation from biotic to abiotic and vice-versa. Thus, our results indicate that these differences might be indistinguishable in fossilized microbialites throughout the geological record.

CONCLUSIONS

Field observations and laboratory analyses from microbial mats of the Maquinchao Basin retrieved in 2015 provide complementary and to some degree opposite results to previous studies performed in microbialites of the area in 2011. We identified diatom rich mats, and similarly to Pacton *et al.* (2015), regular occurrences of SRB along with filaments of unknown origin. Carbonates are observed associated

with erect filamentous in shallow waters locations and active running water whereas the mineral phase is located below OM film in comparatively deeper water areas. Additionally, extrinsic parameters, especially evaporation, might play a more substantial role in the precipitation of these carbonates than previously proposed. However, the environmental differences between 2011 and 2015 in meteorological conditions, regional volcanic activity and associated deposits in the basin might have been responsible of the observed decrease in the mineralization processes, and particularly those associated with photosynthetic activity. Given the changes in morphology of the mats (absence of lamination, low thickness and extent) and lack of photosynthetic organisms detection in the 16S rRNA gene sequence library while SRB were quite numerous, the 2015 Maquinchao microbial mats displayed little primary production and rather substantial organic decay. Our results call for caution when interpreting the degree of the biological impact on the formation of microbialites in the geological record. This is so because local extrinsic factors might have a changeable impact over time switching mineral precipitation from biotic to abiotic and vice-versa. Such switch may or may not be distinguishable in fossilized microbialites.

Acknowledgments

The authors would like to thank E. Carol, F. Campanella, M. Gonzalez Dobra, R. Feo, M. P. Pasquale Perez and F. Suarez for their assistance during different field campaigns, as well as T. Bosco for his laboratory work. Comments and suggestions of two anonymous reviewers have been very helpful improving the final version of the article. This research was funded by the Swiss National Science Foundation (Projects SNF 200021_155927 and 200021_155927/2 to D. Ariztegui).

REFERENCES

Agosta, E., Compagnucci, R., and Ariztegui, D. (2015). Precipitation linked to Atlantic moisture transport: Clues to interpret Patagonian palaeoclimate. *Climate Research*, 62(3): 219–240. https://doi.org/10.3354/cr01272.

Alvarez, M.d.P., Carol, E., Eymard, I., Bilmes, A., and Ariztegui, D. (2021). Hydrochemistry, isotope studies and salt formation in saline lakes of arid regions: Extra Andean Patagonia, Argentina. *Science of the Total Environment.* (https://doi.org/10.1016/j.scitotenv.2021.151529).

Ariztegui, D., Anselmetti, F. S., Gilli, A., and Waldmann, N. (2008). Late Pleistocene Environmental Change in Eastern Patagonia and Tierra del Fuego – A Limnogeological Approach. In J. Rabassa (Ed.), D*evelopments in Quaternary Sciences* 11: 241–253). Elsevier. https://doi.org/10.1016/S1571-0866(07)10011-7

Ariztegui, D., Anselmetti, F. S., Kelts, K., Seltzer, G. O., and D'Agostino, K. (2001). Chapter 14—Identifying Paleoenvironmental Change Across South and North America Using High-Resolution Seismic Stratigraphy in Lakes. In V. Markgraf (Ed.), *Interhemispheric Climate Linkages:* 227–240. Academic Press. https://doi.org/10.1016/B978-012472670-3/50017-3

Arp, G., Reimer, A., and Reitner, J. (2003). Microbialite Formation in Seawater of Increased Alkalinity, Satonda Crater Lake, Indonesia. *Journal of Sedimentary Research*, 73(1): 105–127. https://doi.org/10.1306/071002730105

Awramik, S. M., and Riding, R. (1988). Role of algal eukaryotes in subtidal columnar stromatolite formation. *Proceedings of the National Academy of Sciences*, 85(5): 1327–1329. https://doi.org/10.1073/pnas.85.5.1327

Bilmes, A., D'Elia, L., Lopez, L., Richiano, S., Varela, A., Alvarez, M. del P., Bucher, J., Eymard, I., Muravchik, M., Franzese, J., and Ariztegui, D. (2019). Digital outcrop modelling using "structure-from- motion" photogrammetry: Acquisition strategies, validation and interpretations to different sedimentary environments. *Journal of South American Earth Sciences*, 96: 1-6. https://doi.org/10.1016/j.jsames.2019.102325

Bradbury, J. P., Grosjean, M., Stine, S., and Sylvestre, F. (2001). Chapter 16 - Full and Late Glacial Lake Records Along the PEP 1 Transect: Their Role in Developing Interhemispheric Paleoclimate Interactions. In V. Markgraf (Ed.), *Interhemispheric Climate Linkages*: 265–291. Academic Press. https://doi.org/10.1016/B978-012472670-3/50019-7

Callahan, B. J., McMurdie, P. J., Rosen, M. J., Han, A. W., Johnson, A. J. A., and Holmes, S. P. (2016). DADA2: High-resolution sample inference from Illumina amplicon data. *Nature Methods*, 13(7): 581–583. https://doi.org/10.1038/nmeth.3869

Cartwright, A., Quade, J., Stine, S., Adams, K. D., Broecker, W., and Cheng, H. (2011). Chronostratigraphy and lake-level changes of Laguna Cari-Laufquén, Río Negro, Argentina. *Quaternary Research*, 76(3); 430–440. https://doi.org/10.1016/j.yqres.2011.07.002

Casaburi, G., Duscher, A. A., Reid, R. P., and Foster, J. S. (2015). Characterization of the stromatolite microbiome from Little Darby Island, The Bahamas using predictive and whole shotgun metagenomic analysis. *Environmental Microbiology*, n/a-n/a. https://doi.org/10.1111/1462-2920.13094

Dodds, W. K., Gudder, D. A., and Mollenhauer, D. (1995). The Ecology of Nostoc. *Journal of Phycology*, 31(1): 2–18. https://doi.org/10.1111/j.0022-3646.1995.00002.x

Dupraz, C., Reid, R. P., Braissant, O., Decho, A. W., Norman, R. S., and Visscher, P. T. (2009). Processes of carbonate precipitation in modern microbial mats. *Earth-Science Reviews*, 96(3): 141–162. https://doi.org/10.1016/j.earscirev.2008.10.005

Dupraz, C., Visscher, P. T., Baumgartner, L. K., and Reid, R. P. (2004). Microbe–mineral interactions: Early carbonate precipitation in a hypersaline lake (Eleuthera Island, Bahamas). *Sedimentology*, 51(4): 745–765. https://doi.org/10.1111/j.1365-3091.2004.00649.x

Eymard, I., Alvarez, M. del P., Bilmes, A., Vasconcelos, C., and Ariztegui D (2020). Tracking organomineralization processes from living microbial mats to fossil microbialites. *Minerals*

10: 605 (doi:10.3390/ min10070605).

Eymard, I., Bilmes, A., Alvarez, M. del P., Feo, R., Hunger, G., Vasconcelos, C., and Ariztegui, D. (2019). Growth morphologies and plausible stressors ruling the formation of Late Pleistocene lacustrine carbonate buildups in the Maquinchao Basin (Argentina). *The Depositional Record*, 5(3): 498–514. https://doi.org/10.1002/dep2.81

Farías, M. E., Rascovan, N., Toneatti, D. M., Albarracín, V. H., Flores, M. R., Poiré, D. G., Collavino, M. M., Aguilar, O. M., Vazquez, M. P., and Polerecky, L. (2013). The Discovery of Stromatolites Developing at 3570 m above Sea Level in a High-Altitude Volcanic Lake Socompa, Argentinean Andes. *PLoS ONE*, 8(1): e53497. https://doi.org/10.1371/journal.pone.0053497

Freytet, P., and Verrecchia, E. P. (1998). Freshwater organisms that build stromatolites: A synopsis of biocrystallization by prokaryotic and eukaryotic algae. *Sedimentology*, 45(3): 535–563. https://doi.org/10.1046/j.1365-3091.1998.00155.x

Galloway, R. W., Markgraf, V., and Bradbury, J. P. (1988). Dating shorelines of lakes in Patagonia, Argentina. *Journal of South American Earth Sciences*, 1(2): 195–198. USGS Publications Warehouse. http://pubs.er.usgs.gov/publication/70014176

Gong, J., Myers, K. D., Munoz-Saez, C., Homann, M., Rouillard, J., Wirth, R., Schreiber, A., and van Zuilen, M. A. (2019). Formation and Preservation of Microbial Palisade Fabric in Silica Deposits from El Tatio, Chile. *Astrobiology*, 20(4): 500–524. https://doi.org/10.1089/ast.2019.2025

Lyons, W. B., Long, D. T., Hines, M. E., Gaudette, H. E., and Armstrong, P. B. (1984). Calcification of cyanobacterial mats in Solar Lake, Sinai. *Geology*, 12(10): 623–626. https://doi.org/10.1130/0091-7613(1984)12<623:COCMIS>2.0.CO;2

McMurdie, P. J., and Holmes, S. (2013). phyloseq: An R Package for Reproducible Interactive Analysis and Graphics of Microbiome Census Data. *PLOS ONE*, 8(4): e61217. https://doi.org/10.1371/journal.pone.0061217

Merz-Preiß, M. (2000). Calcification in Cyanobacteria. In R. E. Riding and S. M. Awramik (Eds.), *Microbial Sediments*: 50–56. Springer Berlin Heidelberg. https://doi.org/10.1007/978-3-662-04036-2_7

Merz-Preiß, M., and Riding, R. (1999). Cyanobacterial tufa calcification in two freshwater streams: Ambient environment, chemical thresholds and biological processes. *Sedimentary Geology*, 126: 103–124. https://doi.org/10.1016/S0037-0738(99)00035-4

Pace, A., Bourillot, R., Bouton, A., Vennin, E., Braissant, O., Dupraz, C., Duteil, T., Bundeleva, I., Patrier, P., Galaup, S., Yokoyama, Y., Franceschi, M., Virgone, A., and Visscher, P. T. (2018). Formation of stromatolite lamina at the interface of oxygenic-anoxygenic photosynthesis. *Geobiology*, 16(4): 378–398. https://doi.org/10.1111/gbi.12281

Pacton, M., Hunger, G., Martinuzzi, V., Cusminsky, G., Burdin, B., Barmettler, K., Vasconcelos, C., and Ariztegui, D. (2015). Organomineralization processes in freshwater stromatolites: A living example from eastern Patagonia. *The Depositional Record*, 1(2): 130–146. https://doi.org/10.1002/dep2.7

Pentecost, A. (2005). *Travertine*. Springer Netherlands. //www.springer.com/la/book/9781402035234

Quast, C., Pruesse, E., Yilmaz, P., Gerken, J., Schweer, T., Yarza, P., Peplies, J., and Glöckner, F. O. (2013). The SILVA ribosomal RNA gene database project: Improved data processing and web-based tools. *Nucleic Acids Research*, 41(D1): D590–D596. https://doi.org/10.1093/nar/gks1219

Reid, R. P., Macintyre, I. G., Browne, K. M., Steneck, R. S., and Miller, T. (1995). Modern marine stromatolites in the Exuma Cays, Bahamas: Uncommonly common. *Facies*, 33(1): 1–17. https://doi.org/10.1007/BF02537442

Riding, R. (2011a). Microbialites, Stromatolites, and Thrombolites. In J. Reitner and V. Thiel (Eds.), *Encyclopedia of Geobiology*. Springer Netherlands, 635–654.

Riding, R. (2011b). Calcified Cyanobacteria. In J. Reitner and V. Thiel (Eds.), *Encyclopedia of Geobiology*. Springer Netherlands, 211–223.

Roche, A., Vennin, E., Bundeleva, I., Bouton, A., Payandi-Rolland, D., Amiotte-Suchet, P., Gaucher, E. C., Courvoisier, H., and Visscher, P. T. (2019). The Role of the Substrate on the Mineralization Potential of Microbial Mats in A Modern Freshwater River (Paris Basin, France). *Minerals*, 9(6): 359. https://doi.org/10.3390/min9060359.

Schwalb, A., Burns, S. J., Cusminsky, G., Kelts, K., and Markgraf, V. (2002). Assemblage diversity and isotopic signals of modern ostracodes and host waters from Patagonia, Argentina. *Palaeogeography, Palaeoclimatology, Palaeoecology*, 187(3): 323–339. http://www.sciencedirect.com/science/article/pii/S0031018202004844

Souza-Egipsy, V., Wierzchos, J., Ascaso, C., and Nealson, K. H. (2005). Mg–silica precipitation in fossilization mechanisms of sand tufa endolithic microbial community, Mono Lake (California). *Chemical Geology*, 217(1): 77–87. https://doi.org/10.1016/j.chemgeo.2004.12.004

Takahashi, S., Tomita, J., Nishioka, K., Hisada, T., and Nishijima, M. (2014). Development of a Prokaryotic Universal Primer for Simultaneous Analysis of Bacteria and Archaea Using Next-Generation Sequencing. *PLoS ONE*, 9(8): e105592. https://doi.org/10.1371/journal.pone.0105592

Tatur, A., del Valle, R., Bianchi, M.-M., Outes, V., Villarosa, G., Niegodzisz, J., and Debaene, G. (2002). Late Pleistocene palaeolakes in the Andean and Extra-Andean Patagonia at mid-latitudes of South America. *Quaternary International*, 89(1): 135–150. https://doi.org/10.1016/S1040-6182(01)00085-4

Visscher, P. T., and Stolz, J. F. (2005). Microbial mats as bioreactors: Populations, processes, and products. *Palaeogeography, Palaeoclimatology, Palaeoecology*, 219(1–2): 87–100. https://doi.org/10.1016/j.palaeo.2004.10.016

Wacey, D., Urosevic, L., Saunders, M., and George, A. D. (2018). Mineralisation of filamentous cyanobacteria in Lake Thetis stromatolites, Western Australia. *Geobiology*, 16(2): 203–215. https://doi.org/10.1111/gbi.12272

Waite, D. W., Chuvochina, M., Pelikan, C., Parks, D. H., Yilmaz, P., Wagner, M., Loy, A., Naganuma, T., Nakai, R., Whitman, W. B., Hahn, M. W., Kuever, J., and Hugenholtz, P. (2020). Proposal to reclassify the proteobacterial classes Deltaproteobacteria and Oligoflexia, and the phylum Thermodesulfobacteria into four phyla reflecting major functional capabilities. *International Journal of Systematic and Evolutionary Microbiology*, 70(11): 5972–6016. https://doi.org/10.1099/ijsem.0.004213

Whatley, R. C., and Cusminsky, G. C. (1999). Lacustrine Ostracoda and late Quaternary palaeoenvironments from the Lake Cari-Laufquen region, Rio Negro province, Argentina. Palaeogeography, Palaeoclimatology, Palaeoecology, 151(1–3): 229–239. https://doi.org/10.1016/S0031-0182(99)00022-X